REPORT

Mutations in *TMEM260* Cause a Pediatric Neurodevelopmental, Cardiac, and Renal Syndrome

Asaf Ta-Shma,[1,9] Tahir N. Khan,[2,9] Asaf Vivante,[3,4,9] Jason R. Willer,[2] Pavle Matak,[2] Chaim Jalas,[5] Ben Pode-Shakked,[4,6,7] Yishay Salem,[6,7] Yair Anikster,[6,7] Friedhelm Hildebrandt,[3] Nicholas Katsanis,[2,*] Orly Elpeleg,[8,*] and Erica E. Davis[2]

Despite the accelerated discovery of genes associated with syndromic traits, the majority of families affected by such conditions remain undiagnosed. Here, we employed whole-exome sequencing in two unrelated consanguineous kindreds with central nervous system (CNS), cardiac, renal, and digit abnormalities. We identified homozygous truncating mutations in *TMEM260*, a locus predicted to encode numerous splice isoforms. Systematic expression analyses across tissues and developmental stages validated two such isoforms, which differ in the utilization of an internal exon. The mutations in both families map uniquely to the long isoform, raising the possibility of an isoform-specific disorder. Consistent with this notion, RT-PCR of lymphocyte cell lines from one of the kindreds showed reduced levels of only the long isoform, which could be ameliorated by emetine, suggesting that the mutation induces nonsense-mediated decay. Subsequent in vivo testing supported this hypothesis. First, either transient suppression or CRISPR/Cas9 genome editing of zebrafish *tmem260* recapitulated key neurological phenotypes. Second, co-injection of morphants with the long human *TMEM260* mRNA rescued CNS pathology, whereas the short isoform was significantly less efficient. Finally, immunocytochemical and biochemical studies showed preferential enrichment of the long TMEM260 isoform to the plasma membrane. Together, our data suggest that there is overall reduced, but not ablated, functionality of *TMEM260* and that attenuation of the membrane-associated functions of this protein is a principal driver of pathology. These observations contribute to an appreciation of the roles of splice isoforms in genetic disorders and suggest that dissection of the functions of these transcripts will most likely inform pathomechanism.

Whole-exome and whole-genome sequencing (WES and WGS, respectively) have accelerated the expansion of the repertoire of human loci underscoring Mendelian phenotypes to account for ~3,000 human genes (15%).[1] Nonetheless, the diagnostic yield remains <50%,[2–4] suggesting that the majority of disease-causing lesions are yet to be identified and that a significant fraction of this genetic burden is likely to be contributed by ultra-rare or private mutations. To contribute to the saturation of the morbid human genome as a means of improving both diagnostic value and mechanistic insight, we undertook the systematic sequencing of families affected by suspected genetic disorders, with an emphasis on congenital syndromic traits. Here, we report the genetic and functional dissection of affected individuals with a genetically undiagnosed syndrome characterized by cardiac, CNS, renal, and digit abnormalities in two unrelated consanguineous pedigrees. We show that the likely molecular cause, homozygous truncating mutations in *TMEM260*, affect the functions of one of the two established isoforms transcribed from this locus, thereby demonstrating the necessity of the long isoform for the development of multiple tissues.

We consulted family 1, a consanguineous Ashkenazi Jewish pedigree, who had experienced three recurrent births with cardiac complications that resulted in perinatal lethality in two of the three children (Figure 1A). Male and female individuals 1-II-1 and 1-II-2, respectively, were born at term and presented with central cyanosis and heart murmur shortly after birth. Echocardiography of 1-II-1 revealed a complex heart defect including truncus arteriosus, a ventricular septal defect (VSD), an interrupted aortic arch, and a partial anomalous pulmonary venous return. Similarly, clinical imaging of individual 1-II-2 revealed notable cardiac defects that included tricuspid valve atresia, truncus arteriosus type I with severe truncal valve stenosis and moderate regurgitation, a VSD, a right aortic arch, and persistent left superior vena cava to coronary sinus. Brain ultrasound of individuals 1-II-1 and 1-II-2 showed partial agenesis of the corpus callosum. During the first days of life, both infants developed generalized edema along with high creatinine levels (>1.3 mg/dL; normal: 0.2–0.9 mg/dL). After corrective cardiac surgery, individual 1-II-1 did not recover and suffered from severe anasarca secondary to a massive capillary leak, deteriorating renal failure, and oliguria. This led to multi-organ failure and death at the age of 2 months. Individual 1-II-2, in addition to the heart and brain malformations, displayed a webbed neck, postaxial polydactyly of the left hand, low-set ears, and bilateral preauricular skin tags. She passed away at the age of 6 weeks from cardiac and pulmonary failure. A third affected child,

[1]Department of Pediatric Cardiology, Hadassah Medical Center, Jerusalem 91120, Israel; [2]Center for Human Disease Modeling, Duke University Medical Center, Durham, NC 27701, USA; [3]Department of Medicine, Boston Children's Hospital and Harvard Medical School, Boston, MA 02115, USA; [4]Talpiot Medical Leadership Program, Sheba Medical Center, Tel-Hashomer, Ramat Gan 52621, Israel; [5]Bonei Olam, Center for Rare Jewish Genetic Disorders, Brooklyn, NY 11204, USA; [6]Edmond and Lily Safra Children's Hospital, Sheba Medical Center, Tel-Hashomer, Ramat Gan 52621, Israel; [7]Sackler Faculty of Medicine, Tel-Aviv University, Tel-Aviv 6997801, Israel; [8]Monique and Jacques Roboh Department of Genetic Research, Hadassah Medical Center, Jerusalem 91120, Israel
[9]These authors contributed equally to this work
*Correspondence: katsanis@cellbio.duke.edu (N.K.), elpeleg@hadassah.org.il (O.E.)
http://dx.doi.org/10.1016/j.ajhg.2017.02.007.

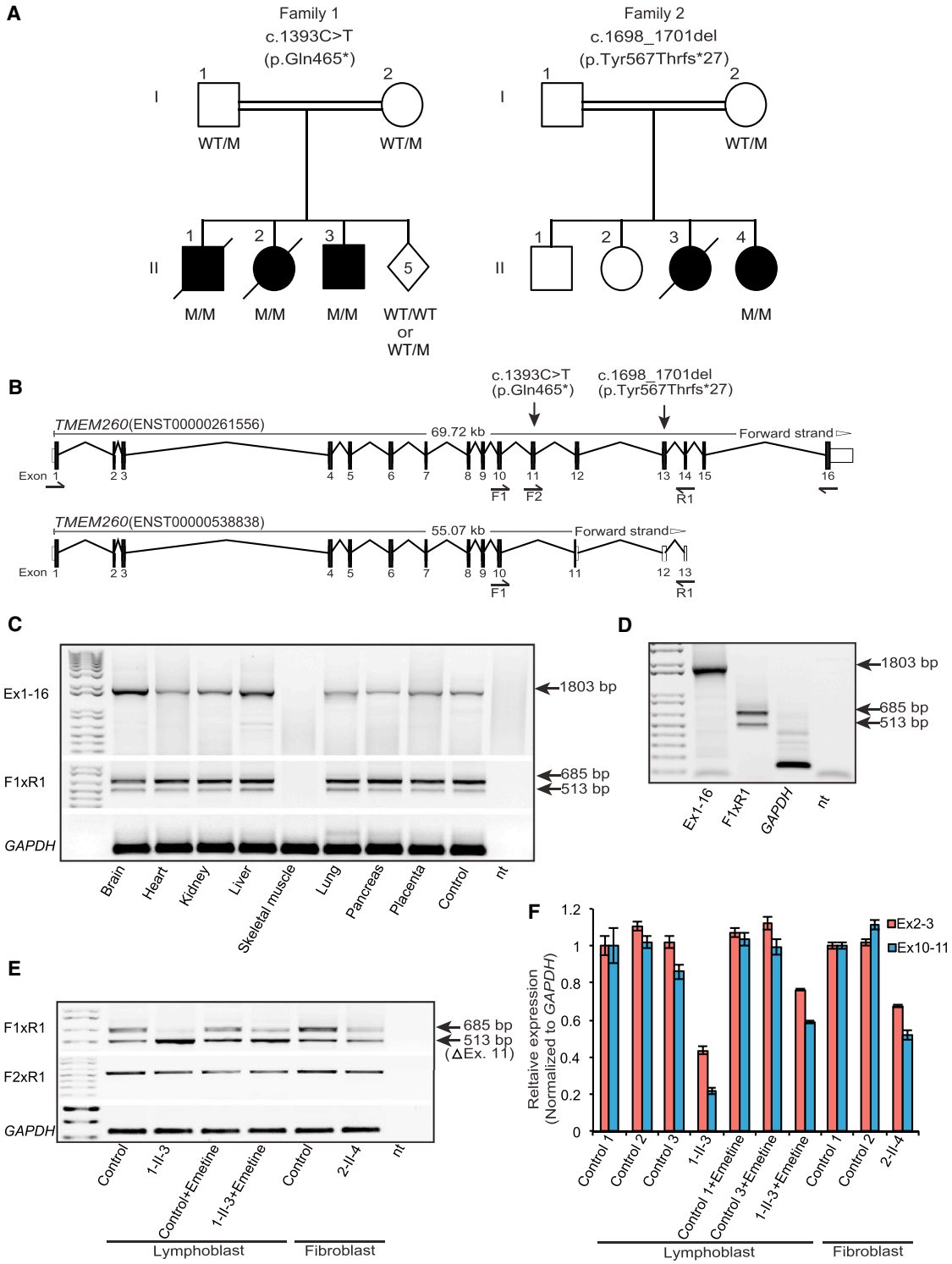

Figure 1. Homozygous Truncating Mutations in *TMEM260* Result in a Reduction of the Canonical Transcript

(A) Two unrelated consanguineous pedigrees affected by *TMEM260* mutations. Family 1 (left) has three affected individuals (1-II-1, 1-II-2, and 1-II-3) who harbor a homozygous *TMEM260* truncating mutation that segregates with disease (c.1393C>T [p.Gln465*]). Five healthy siblings are either wild-type (WT) or heterozygous for the mutation (M). A single affected individual (2-II-4) from an unrelated pedigree (family 2) has a homozygous truncating mutation in *TMEM260* (c.1698_1701del [p.Tyr567Thrfs*27]). Affected individuals are indicated with filled squares (male) and circles (female), unaffected individuals are indicated by unfilled squares (male) and circles (female), and diagonal lines indicate deceased individuals.

(B) Schematic of the human *TMEM260* locus shows the position of the two truncating mutations found in families 1 and 2. *TMEM260* has two protein-coding isoforms (long [top] and short [bottom]), but both mutations affect only the long isoform. c.1393C>T is located in exon 11 of the long transcript but is not present in the short transcript. c.1698_1701del (p.Tyr567Thrfs*27) is in the protein-coding part of the long transcript but in the 3′ UTR of the short transcript.

(legend continued on next page)

individual 1-II-3, was a full-term male baby who presented with systolic murmur due to VSDs and atrial septal defects (ASDs). Upon physical examination, we noted facial port wine nevus, an overriding fourth left toe, and an undescended right testis. Abdominal ultrasound demonstrated multiple small left renal cysts. The VSDs closed spontaneously during the first year of life; at the last clinical assessment (2 years), he had a small ASD (Table 1; Supplemental Note).

Independently, we consulted family 2, an Arabic pedigree with a neonate referred as a result of a cyanotic heart defect diagnosed at birth (Figure 1A). Individual 2-II-4 (CK429_AN31_21) was born at term to consanguineous parents (double first-degree cousins) after an uncomplicated pregnancy. She presented initially at the age of 2 weeks with cyanosis, significant total body edema, and vomiting during feeding. On physical examination, we noted a 2/6 systolic murmur; an echocardiogram revealed tetralogy of Fallot with pulmonic atresia. A neurological examination revealed microcephaly and hypotonia, but head ultrasound was normal. Renal ultrasound showed that both kidneys were at the upper range of normal; however, the pyramids appeared echogenic in both kidneys. These findings were accompanied by persistently elevated creatinine levels (1.93 mg/dL; normal: 0.2–0.9 mg/dL). After surgery, individual 2-II-4 was stable and discharged. However, 1 year later, she passed away suddenly at home. The family history is positive for a female sibling (2-II-3) who died at the age of 35 days as a result of congenital heart disease. Individual 2-II-4 has two older living siblings, a 6-year-old male (2-II-1) and a 5-year-old female (2-II-2), with no reported congenital malformations but with seizures and intellectual disability, respectively (Table 1; Supplemental Note).

On the basis of the recurrence of similar clinical features, non-gender bias for the incidence of disease, and reportedly healthy parents, we hypothesized an autosomal-recessive mode of inheritance in both families. To investigate the molecular underpinnings of disease in family 1, we collected DNA samples after obtaining informed consent and approval from the review board at Hadassah Medical Center, and we conducted WES of both parental samples (sufficient DNA quantities were unavailable from individuals 1-II-1 and 1-II-2 for WES). We generated capture libraries by using the SureSelect Human All Exon 50 Mb Kit (V4, Agilent Technologies) and obtained 100 bp paired-end reads on a HiSeq 2000 instrument (Illumina) with a mean of 57× coverage across the two samples (Table S1) as previously described.[5] We aligned WES data to the human reference genome (UCSC Genome Browser hg19; GRCh37) and called variants by using the DNAnexus platform with default parameters. Of the variants called, we narrowed candidates according to the following strategy: (1) retention of only heterozygous variants present in both parents, (2) quality score > 30, (3) read depth > 10×, (4) functional variants altering coding regions and splice junctions, (5) <1% minor allele frequency (MAF) in the 60,000 exomes from the Exome Aggregation Consortium (ExAC) Browser,[6] and (6) <3% MAF in our in-house exome dataset (~600 Ashkenazi Jewish individuals). This filtering strategy resulted in 22 rare variants (Tables S2 and S3); among these, we excluded seven variants residing in genes implicated in human genetic disorders not consistent with the phenotype or inheritance pattern of family 1. Of the remaining 15 rare variants, we prioritized the sole nonsense variant in exon 11 of *TMEM260* (GenBank: NM_017799.3; c.1393C>T [p.Gln465*]) for segregation by using Sanger sequencing (Table S4). We confirmed that both parents were heterozygous, the affected siblings were each homozygous at this site, and five unaffected siblings were either wild-type (WT) or heterozygous carriers (Figure 1A). *TMEM260* c.1393C>T is not present in the homozygous state in the ExAC Browser and, at a frequency of 9/60,052 heterozygous individuals (including non-Finnish Europeans), is ultra-rare.

For family 2 (Figure 1A), we collected blood samples and pedigree information from the affected individual (2-II-4) and his mother after obtaining informed consent and analyzed them as previously described.[7,8] Approval for human subject research was obtained from the institutional review boards of Tel HaShomer Hospital and Boston Children's Hospital. We captured genomic DNA with an Agilent SureSelect All Exome Kit v.2.0 (Agilent Technologies) and sequenced the library on a HiSeq instrument (Illumina) to obtain a mean target coverage of 45× (Table S1). We performed all subsequent sequence alignment to the reference human genome (hg19) and variant calling by using CLC Genomics Workbench (v.6.5.1) software (CLC bio). First,

(C and D) RT-PCR analyses of *TMEM260* across eight different human tissues (Clontech Human MTC Panel I) (C) and a mixture of 35 different human tissues pooled from various developmental stages (Clontech Human Universal QUICK-Clone II) (D) show the presence of the long transcript (sequence confirmed) when amplified with primers located in exons 1 and 16 of the annotated long transcript. In contrast, amplification with primers F1 and R1 (located in exons 10 and 14, respectively) shows the presence of both long and short transcripts (sequence confirmed). *GAPDH* was used to control for RNA integrity.
(E) Qualitative RT-PCR analysis from a lymphocyte cell line established from individual 1-II-3 and a primary fibroblast cell line isolated from individual 2-II-4 shows less expression of the long transcript than in the control, whereas the short transcript remains unaffected. Agarose gel images are shown; F1, F2, and R1 are the primers (located in exons 10, 11, and 14, respectively) depicted in (B), and *GAPDH* was used to control for RNA integrity.
(F) qPCR (40 cycles of amplification) from the lymphoblastoid cell line of individual 1-II-3 shows significantly less expression (~5-fold reduction; $p = 0.001$) of the long *TMEM260* transcript than in lymphoblast control 1; this is rescued by the addition of emetine to the culture medium (~3-fold increase; $p = 0.006$ versus individual 1-II-3). qPCR from a fibroblast cell line of individual 2-II-4 shows less expression (~2-fold reduction; $p = 0.05$) of the long *TMEM260* long than in fibroblast control 1. Experiments were performed in triplicate and normalized to *GAPDH* expression.

Table 1. Clinical Phenotypes of Affected Individuals with *TMEM260* Mutations

	1-II-1	1-II-2	1-II-3	2-II-4
Age	deceased (2 months)	deceased (6 weeks)	2 years	deceased (1 year)
Mutation	c.1393C>T (p.Gln465*)	c.1393C>T (p.Gln465*)	c.1393C>T (p.Gln465*)	c.1698_1701del (p.Tyr567Thrfs*27)
Cardiac Defects				
Septal defect(s)	VSD	VSD	VSD, ASD	VSD
Systolic murmur	+	+	+	+
Truncus arteriosus	+	+	–	–
Tetralogy of Fallot, pulmonic atresia, and major aortopulmonary collateral arteries	–	–	–	+
Interrupted aortic arch	+	–	–	–
Right aortic arch	–	+	–	–
Tricuspid valve atresia	–	+	–	–
Persistent left superior vena cava	–	+	–	–
Partial anomalous pulmonary venous return	+	–	–	–
CNS Defects				
Agenesis of corpus callosum	+	+	–	NA
Microcephaly	–	–	–	+
Renal Defects				
Creatinine levels (normal: 0.2–0.9 mg/dL)	elevated (1.3 mg/dL)	elevated (1.3 mg/dL)	NA	elevated (1.93 mg/dL)
Urine output	oliguria	anuria	–	–
Renal cysts	–	–	+	–
Limb Defects				
Polydactyly	–	+	–	–
Overriding toes	–	–	+	–
Other				
Additional symptoms	generalized edema	edema, cyanosis, low-set ears, bilateral preauricular skin tags, webbed neck	facial port wine nevus, undescended right testis	generalized edema, cyanosis, facial dysmorphism, hypotonia

Abbreviations are as follows: +, present; –, absent; VSD, ventricular septal defect; ASD, atrial septal defect; and NA, not available.

we conducted homozygosity mapping. Downstream processing of aligned BAM files was carried out with Picard and SAMtools;[9] single-nucleotide variants were called with the Genome Analysis Toolkit,[10] and the subsequent VCF file was used in the homozygosity mapper[11] as previously described.[12] We observed 370 Mb of homozygosity, which was distributed in 29 regions ranging in size from 2 to 88 Mb (Figure S1). Next, we used the Integrated Genomics Viewer to filter the WES data according to MAF (<1% in the ExAC Browser), quality ($Q \geq 30$), intersection with homozygous regions, and visual inspection (Table S5). Rare functional variants were present in five genes (Table S6), all of which were Sanger confirmed in individual 2-II-4 and her asymptomatic mother (Table S4). Heterozygous variants in two of the five genes have been implicated previously in disorders with non-overlapping phenotypes. Of the remaining three genes harboring candidate variants, we obtained a phenotype match between *TMEM260* (GenBank: NM_017799.3; c.1698_1701del [p.Tyr567Thrfs*27]) and family 1 by using GeneMatcher.[13]

TMEM260, also known as *C14orf101*, encodes a predicted transmembrane protein of unknown function. Although *TMEM260* has a single validated RefSeq transcript encoding a 707 amino acid polypeptide (GenBank: NM_017799.3 and NP_060269.3; referred to as the long isoform), we noted multiple predicted splice isoforms, one of which we considered potentially relevant to our exome findings. Specifically, we noted an isoform that encodes 409 amino acids (GenBank: BC121163.1 and AAI21164.1; referred to as the short isoform). Alternative splicing of the short isoform

lacks the sequence corresponding to exon 11 of the long transcript, as well as part of the C-terminal coding region of the long isoform (Figures 1B and 3A). The reason for its potential candidacy was that in family 1, the homozygous nonsense mutation, c.1393C>T (p.Gln465*), maps to exon 11 of the long transcript (Figure 1B). Further, the truncating mutation in family 2 (c.1698_1701del [p.Tyr567Thrfs*27]) maps to exon 13, which is also used uniquely by the long isoform of this locus (Figure 1B).

Given these observations, we hypothesized that dysfunction of this isoform might contribute to the disorder. However, given the potentially complex splicing nature of this locus, we first tested the physiological relevance of all computationally predicted transcripts. We amplified the long canonical transcript of *TMEM260* in cDNA obtained from a commercially available panel of eight different human tissues (Clontech Human MTC Panel I) with PCR primers located in exons 1 and 16, and we noted the presence of only one product in seven of eight tissues (Figure 1C, top). Subsequent Sanger sequencing confirmed that the sequence of the amplified product corresponds to the long transcript of *TMEM260*. To investigate the presence of the short *TMEM260* transcript, we amplified the *TMEM260* locus in the aforementioned eight different human tissues from exon 10 to exon 14 and predicted to be shared by multiple transcripts. However, we detected only two products (Figure 1C, middle), sequencing of which confirmed them to be the long and short *TMEM260* transcripts. To test whether some of the additional predicted transcripts might be expressed in a spatiotemporal context not represented in our initial panel, we performed a similar RT-PCR and sequencing experiment in a mix of 35 human tissues collected across various developmental stages (Clontech Human Universal QUICK-Clone II). Once again, the only two transcripts detectable were the aforementioned long and short isoforms (Figure 1D).

Although we cannot exclude the possibility that some of the additional predicted transcripts might be expressed but beyond our detection threshold levels (or have a narrow spatiotemporal expression level that we did not test), our expression data argued that the locus produces two major isoforms, one of which is affected positionally by the mutations we discovered in the two families. As a first test of this hypothesis, we established a lymphoblast cell line from individual 1-II-3. We then extracted total RNA with the RNeasy Mini Kit (QIAGEN) and performed quantitative PCR (qPCR) of the resulting cDNA generated with the Quantitect Reverse Transcription Kit (QIAGEN) and Power SYBR Green PCR Master Mix (Applied Biosystems). Compared with an ethnically matched control individual (lymphoblast control 1), individual 1-II-3 showed ~5-fold less message, given that primers specific to the long isoform annealed to exons 10 and 11 ($p = 0.001$; Table S4); qualitative analysis conducted by amplification of both isoforms concurrently with primers in shared exons (exons 2 and 3), however, showed that the short isoform remained intact in individual 1-II-3 (Figures 1E and 1F). To assess possible expression bias across reactions, we also tested three independent, ethnically matched controls (lymphoblast controls 1–3); we did not observe significant differences in *TMEM260* expression (Figure 1F). We observed further that treatment with emetine led to significantly more expression of the long isoform in lymphoblast cells from individual 1-II-3 than in untreated lymphoblast cells from individual 1-II-3 ($p = 0.006$; Figures 1E and 1F). Together, these data suggest that mutated *TMEM260* product is subjected to nonsense-mediated decay in individual 1-II-3.

We also assessed the relative ratios of the *TMEM260* splice isoforms in family 2. For this purpose, we evaluated mRNA expression in primary fibroblasts from individual 2-II-4 by using an RT-PCR strategy similar to that used with family 1. Both long and short transcripts were detectable, suggesting that the mutation confers no appreciable effect on mRNA stability (Figure 1E). However, qPCR analysis showed 2-fold less expression of the long isoform in individual 2-II-4 than in a tissue-matched control (fibroblast control 1; Figure 1F). Between two tissue-matched controls (fibroblast controls 1 and 2), we did not observe a significant difference in *TMEM260* expression (Figure 1F). These data suggest that, by virtue of their location in the long-isoform-specific C-terminal region, both *TMEM260* mutations affect only the long isoform, whereas the short isoform remains intact.

We and others have demonstrated previously the utility of zebrafish models in testing the candidacy of rare mutations in syndromic disorders;[14–21] this approach includes an experimental paradigm in which expression of mutations in the context of spliced isoforms can be used for testing the specific effect of such alleles.[14,22–24] For TMEM260, we utilized this approach to ask (1) whether the transient suppression or introduction of deletions at the locus can reproduce key aspects of the human pathology, (2) whether the two known isoforms of the human locus might have different abilities to rescue relevant phenotypes, and (3) whether the long *TMEM260* isoform harboring individual 2-II-4's mutation (c.1698_1701del) has the ability to rescue relevant phenotypes.

For evolutionary analysis, we aligned full-length TMEM260 amino acid sequences of human and 22 other vertebrate species available in UniProt. The resulting phylogenetic tree generated with Clustal Omega multiple-sequence alignment showed that TMEM260 is almost ubiquitously present across vertebrate evolution (Figure S2). Reassuringly, the amino acid sequence corresponding to exon 11 is conserved across species (Figure S3A) with 59% similarity to the equivalent exon in zebrafish Tmem260 (Figure S3B). For our in vivo work, we first identified a single *tmem260* ortholog (Ensembl: ENSDART00000154660 [GRCz10]; 48% similarity to human *TMEM260*; Figures S4A and S4B), which we could detect by RT-PCR in 2 day post fertilization (dpf) embryos (Figure S4B). In contrast to human transcripts, a single amplified transcript encodes a full-length protein

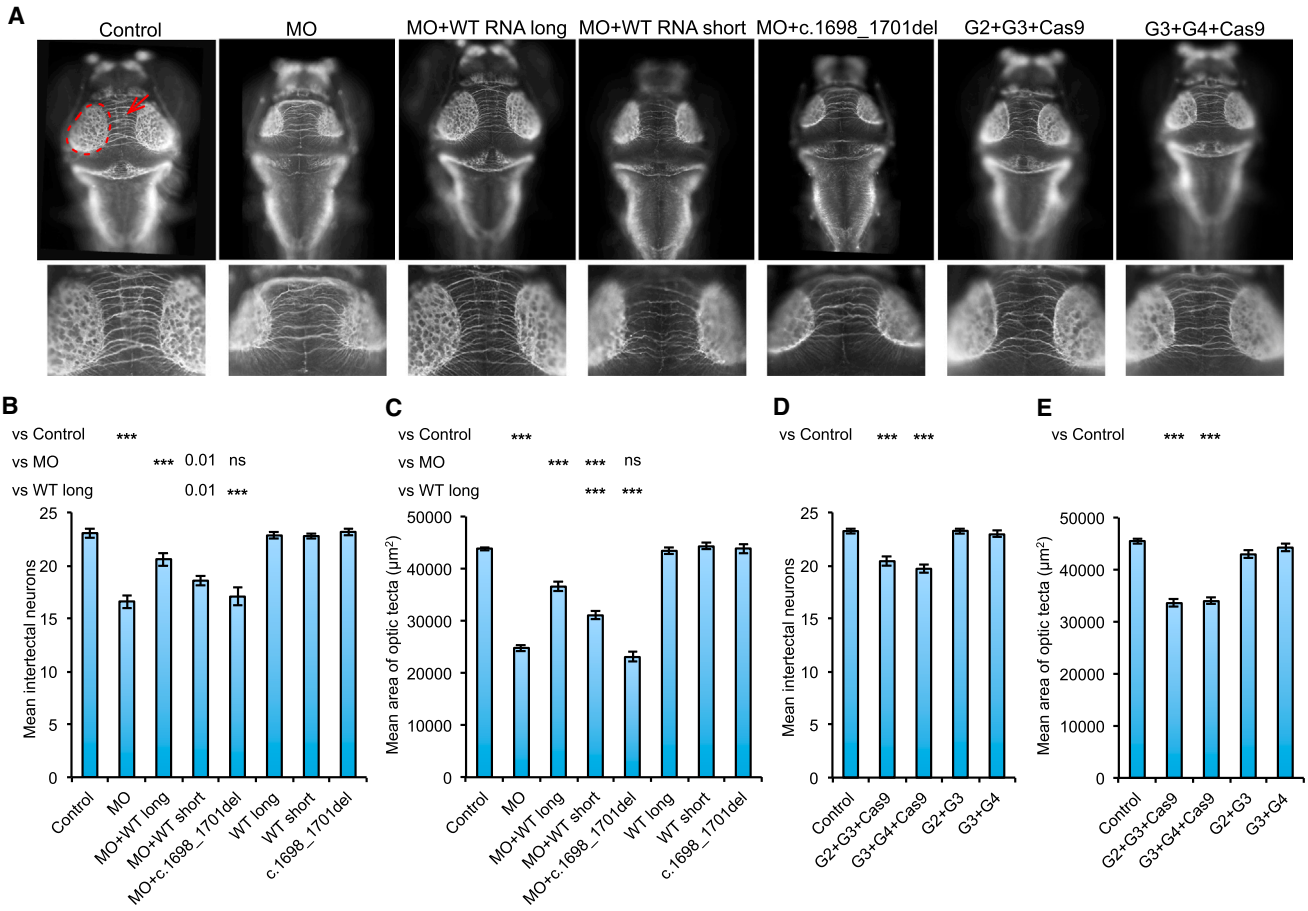

Figure 2. Suppression and Mutation of *tmem260* Results in CNS Defects

(A) Acetylated tubulin staining of WT (ZDR strain) larvae shows brain structures at 3.5 dpf (dorsal view). MOs (second from left) show fewer intertectal neurons (arrow) and smaller optic tecta size (dotted oval).

(B and C) Co-injection of *tmem260* translation-blocking MO and WT long *TMEM260* mRNA rescues intertectal neuron count (B; see zoomed images in the second row of A) and optic tecta size. Co-injection of *tmem260* MO and WT short *TMEM260* mRNA rescues intertectal neuron count (B) and optic tecta size (C) but less significantly than co-injection of MO and WT long *TMEM260* mRNA (n = 52–74 larvae per batch, repeated). Co-injection of *tmem260* MO and WT long *TMEM260* mRNA harboring c.1698_1701del does not rescue intertectal neuron count (B) or optic teca size (C) (n = 37–39 larvae per batch, repeated).

(D and E) CRISPR/Cas9 F0 mutants (A: sixth and seventh from left) show significantly fewer intertectal neurons (D) and smaller optic tecta size (E). G2, G3, and G4 are CRISPR guide RNAs 2, 3, and 4, respectively. n = 48 larvae per batch, repeated. ***$p < 0.0001$; ns, not significant (Student's t test). Error bars indicate SEM.

of 684 amino acids (Figures S4A and S4B); this transcript is also localized to anterior structures (9.5 counts per million mapped reads in 5 dpf zebrafish heads; GEO: GSE63191).[14]

We designed a translation-blocking morpholino (MO; Table S4) and injected increasing doses into WT embryos (ZDR strain, Aquatica BioTech) at the 1- to 4-cell stage. All zebrafish studies were approved by the Duke University Institutional Animal Care and Use Committee. We focused primarily on modeling CNS defects of the affected individuals (microcephaly and agenesis of the corpus callosum), for which there are well-described proxies in zebrafish: optic tecta are bilateral oval structures occupying a major portion of the midbrain, and the area is an indicator of head size.[14] Further, we were able to image (and count) the neurons connecting the midbrain hemispheres, a proxy for the corpus callosum in humans. Staining with a mouse anti-acetylated α-tubulin antibody (Sigma T7451; 1:1,000 dilution), followed by image acquisition and quantitative measurement as previously described,[14,15] revealed significantly smaller optic tecta size and fewer intertectal neurons in 3.5 dpf morphants than in uninjected controls (Figures 2A–2C). Co-injection of WT long *TMEM260* mRNA and MO resulted in significant rescue of both CNS abnormalities (n = 52–74 larvae per batch; $p < 0.0001$; repeated with masked scoring; Figures 2A–2C). Co-injection of short *TMEM260* mRNA and MO also improved optic tecta size and intertectal neuron count. However, both phenotypic readouts were still significantly worse than that of long *TMEM260* mRNA (Figures 2A–2C; $p < 0.0001$ for optic tecta size; $p = 0.01$ for intertectal neurons), suggesting that short *TMEM260* mRNA confers partial functionality. To test the second discovered allele, we co-injected MO and long *TMEM260* mRNA harboring

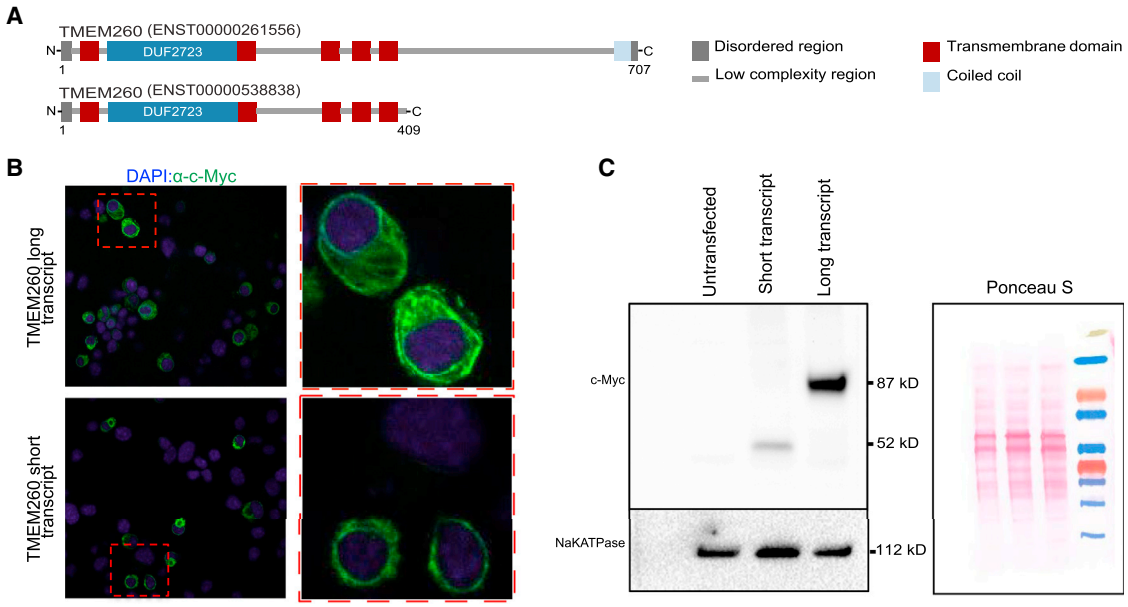

Figure 3. Truncation of TMEM260 Inhibits Proper Localization to Cellular Membranes
(A) Predicted structure of the long and short forms of TMEM260, including the arrangement of domains.
(B) Immunostaining of Neuro2A cells transfected with TMEM260 c-Myc-tagged long (top) and short (bottom) isoforms.
(C) Immunoblot (left) and Ponceau S loading control (right) show the relative concentration of c-Myc-tagged long (87 kDa) and short (52 kDa) isoforms of TMEM260 in the membrane lysates (as indicated by Na^+/K+ ATPase IB; bottom) of transiently transfected Neuro2A cells.

c.1698_1701del. Consistent with our prediction, this message did not rescue CNS abnormalities (n = 37–39 larvae per batch; $p < 0.0001$, replicated; Figures 2A–2C), suggesting loss of WT function. Ectopic expression of long, short, and c.1698_1701del *TMEM260* mRNA did not produce any significant CNS abnormalities (Figures 2B and 2C).

In addition to the rescue experiments, we tested the specificity of the phenotype by generating deletions in the zebrafish locus with CRISPR/Cas9-mediated genome editing. We designed and validated three CRISPR guide RNAs (G2, G3, and G4; Table S4) targeting exons 2, 7, and 5 of *D. rerio tmem260*, respectively, according to previously described methods,[16] and we injected guide RNA and Cas9 into single-cell embryos (n = 48–74 embryos per batch). We established the efficiency of each reagent by genomic DNA isolation, heteroduplex detection on 15% polyacrylamide gel electrophoresis (n = 6 embryos tested per condition),[25] and subsequent cloning and sequencing of PCR amplicons to estimate mosaicism. We observed an average of 45%–75% mosaicism for each of the three guide RNAs independently (n = 3 embryos assessed per condition; Figures S4D–S4I). We then injected CRISPR guides in pairwise combinations (100 pg per guide RNA) with Cas9 (200 pg; PNA Bio). We found a significant reduction in the number of intertectal neurons (Figure 2D) as well as size of the optic tecta (Figure 2E) in 3.5 dpf zebrafish larvae injected with either a G2-G3-Cas9 or G3-G4-Cas9 combination ($p < 0.0001$; n = 48–74 embryos per condition, replicated). Injection of equivalent doses of guide RNA in the absence of Cas9 did not result in any phenotypes (Figures 2D and 2E). Together, our in vivo data show recapitulation of the anatomical phenotypes observed in affected children with truncating *TMEM260* mutations and demonstrate that the short isoform is insufficient to fully compensate for the loss of the long isoform's function.

Given these observations, we wondered whether the disparate C-terminal coding regions of each of the TMEM260 isoforms conferred differential protein localization that could possibly be linked to varying function. To investigate the cellular localization of the two TMEM260 proteins, we generated pCS2+ expression constructs with an N-terminal c-Myc epitope tag (6× EQKLISEEDL) corresponding to each of the long and short WT open reading frames. We seeded murine Neuro2a cells on coverslips in 6-well plates and transfected transiently with short and long TMEM260 isoform constructs by using DharmaFECT (Dharmacon) according to the manufacturer's instructions. Two days after transfection, we fixed cells with 4% paraformaldehyde for immunocytochemical analysis by using c-Myc (Sigma M4439; 1:500 dilution) and Alexa Fluor-488 (Molecular Probes, ThermoFisher; 1:500 dilution) primary and secondary antibodies, respectively. We mounted coverslips on glass slides with DAPI-containing Fluoro Shield solution (Calbiochem) and acquired fluorescent signals on a Nikon 90i microscope with a confocal head.

We observed clear differences in subcellular distribution between the two isoforms. For the long isoform, there was uniform protein distribution throughout the cytoplasm and appreciable localization in the vicinity of the plasma membrane; in contrast, the protein encoded by the short isoform was largely perinuclear (Figure 3B). Given the

quantitative limitations of immunocytochemistry, we performed biochemical localizations studies, in which we fractionated cells in high sucrose buffer as previously described,[26] purified membrane fractions, and performed immunoblotting either with the Myc tag or with an antibody against Na^+/K+ ATPase, a membrane marker (Abcam ab7671; 1:10,000 dilution). In this experiment, we observed a striking difference in the relative ratios of long and short protein isoforms in the membrane (Figure 3C), a result consistent with the observed immunocytochemical distributions.

Here, we have shown that truncating mutations in *TMEM260* cause a syndrome characterized by CNS, cardiac, renal, and axial skeletal defects. Notably, the homozygous truncating mutations found in both our families affected specifically one of the two splice isoforms generated by this locus, arguing specificity in the phenotypic driver. Consistent with this notion, the long isoform is significantly more efficient than the short isoform in rescuing CNS anomalies in a zebrafish model of this disorder. We note the need for caution in interpreting this result given that the zebrafish *tmem260* ortholog does not appear to encode the short isoform. However, the partial rescue observed with the short human isoform argues that this isoform is functional in zebrafish embryos. Still, we do not know whether the differential rescue of the CNS pathologies by the two splice isoforms is also true for other related phenotypes.

As part of our studies, we also assessed the heart, kidneys, and fin in our zebrafish morphants and observed pathologies relevant to the human disease (pericardial edema, kidney filtration defect, and blunted pectoral fins in a dose-dependent manner and reduced renal convolution at high doses; Figure S5). We note that we were able to recapitulate pericardial edema and kidney filtration defects (evident by proteinuria) in CRISPR F0 mutants (Figures S5A, S5D, S5E, and S5H). We were not able to rescue these phenotypes, and thus we cannot be confident of their specificity; nonetheless, we also observed a dose-dependent pericardial edema (Figures S5A and S5C) in larvae when a second MO (sb MO; Figure S4C) was injected at increasing concentrations, arguing that the failed rescue with human mRNA might possibly be due to cross-species differences rather than non-specificity of the phenotype. In that context, the future characterization of F2 mutants might be helpful.

Conservative estimates indicate that the TMEM domain is found in 13% of the proteome.[27] Unsurprisingly, there are numerous examples of variant TMEM proteins in human genetic disorders,[28–34] and in that context, we do gain pathomechanistic clues about the disorder. We have reported enrichment of TMEM domains in the ciliary proteome,[35] raising the possibility that the present constellation of phenotypes could be part of the ciliopathy spectrum.[36] However, staining for cilia in fibroblasts from affected individuals did not reveal any appreciable structural defects (Figure S6), suggesting that either ciliary function is normal or the cell type and/or type of ciliary defect that drives pathology could not be appreciated with the available cells and experimental paradigm. As such, agnostic methods that include transcriptomic and proteomic studies of cells and model organisms might be necessary for gaining further insight.

Finally, our observations potentially contribute to a growing list of genetic disorders caused by isoform-specific mutations and highlight the utility of the zebrafish model in dissecting such phenomena. For example, mutations specifically affecting the cytoplasmic functions of *DNAJB6* cause limb-girdle muscular dystrophy (OMIM: 611332 and 603511) by increasing the half-life (and toxicity of the isoform),[24] whereas *MEIS1* (OMIM: 601739) mutations that affect one of the splice isoforms of that locus predispose to restless leg syndrome (OMIM: 612853), most likely through a subcellular distribution mechanism.[23] We cannot exclude the formal possibility that the *TMEM* locus generates additional transcripts that were not detectable by our experimental paradigm. However, the presence of two transcripts in the major organs affected by the disorder and the fact that the discovered mutations appear to affect the function of one transcript represent evidence of likely isoform specificity. We speculate that mutations that affect both transcripts might be incompatible with life and that dissecting potentially different functions for the two TMEM260 isoforms will thus be of value in understanding pathomechanism. Our immunocytochemical and biochemical studies propose some initial clues: even though both isoforms are predicted to encode several transmembrane domains, only the long isoform can be appreciated substantially in the membrane. These data argue that the C termini of the protein might confer subcellular localization specificity or indeed a discrete functionality in one of the organellar membranes and merit further exploration.

Supplemental Data

Supplemental Data include a Supplemental Note, six figures, and six tables and can be found with this article online at http://dx.doi.org/10.1016/j.ajhg.2017.02.007.

Conflicts of Interest

N.K. is a paid consultant for and holds significant stock of Rescindo Therapeutics, Inc.

Acknowledgments

We thank Dr. Jeffrey Jacobson from Edmond and Lily Safra Children's Hospital (Israel) for his technical assistance. This work was funded by US NIH grants DK075972, HD042601, and DK096415 (N.K.), DK072301 and DK096493 (N.K. and E.E.D.), MH106826 (E.E.D.), and DK068306 (F.H.) and the Trudy Mandel Louis Charitable Trust (O.E.). N.K. is a distinguished Jean and George Brumley Professor. F.H. is the William E. Harmon Professor. A.V. is supported by grants from the Manton Center Fellowship program, Boston Children's Hospital, and the Mallinckrodt Research Fellowship Award.

Received: August 12, 2016
Accepted: February 17, 2017
Published: March 16, 2017

Web Resources

DNAnexus, https://www.dnanexus.com/
Exome Aggregation Consortium (ExAC) Browser, http://exac.broadinstitute.org
GenBank, http://www.ncbi.nlm.nih.gov/genbank/
GeneMatcher, https://genematcher.org/
Ensembl, https://ensembl.org
Gene Expression Omnibus, http://www.ncbi.nlm.nih.gov/geo/
OMIM, http://www.omim.org
Pfam, http://pfam.xfam.org/
UniProt, http://www.uniprot.org/

References

1. Chong, J.X., Buckingham, K.J., Jhangiani, S.N., Boehm, C., Sobreira, N., Smith, J.D., Harrell, T.M., McMillin, M.J., Wiszniewski, W., Gambin, T., et al.; Centers for Mendelian Genomics (2015). The Genetic Basis of Mendelian Phenotypes: Discoveries, Challenges, and Opportunities. Am. J. Hum. Genet. *97*, 199–215.
2. Yang, Y., Muzny, D.M., Reid, J.G., Bainbridge, M.N., Willis, A., Ward, P.A., Braxton, A., Beuten, J., Xia, F., Niu, Z., et al. (2013). Clinical whole-exome sequencing for the diagnosis of mendelian disorders. N. Engl. J. Med. *369*, 1502–1511.
3. Lee, H., Deignan, J.L., Dorrani, N., Strom, S.P., Kantarci, S., Quintero-Rivera, F., Das, K., Toy, T., Harry, B., Yourshaw, M., et al. (2014). Clinical exome sequencing for genetic identification of rare Mendelian disorders. JAMA *312*, 1880–1887.
4. Soden, S.E., Saunders, C.J., Willig, L.K., Farrow, E.G., Smith, L.D., Petrikin, J.E., LePichon, J.B., Miller, N.A., Thiffault, I., Dinwiddie, D.L., et al. (2014). Effectiveness of exome and genome sequencing guided by acuity of illness for diagnosis of neurodevelopmental disorders. Sci. Transl. Med. *6*, 265ra168.
5. Perles, Z., Moon, S., Ta-Shma, A., Yaacov, B., Francescatto, L., Edvardson, S., Rein, A.J., Elpeleg, O., and Katsanis, N. (2015). A human laterality disorder caused by a homozygous deleterious mutation in MMP21. J. Med. Genet. *52*, 840–847.
6. Lek, M., Karczewski, K.J., Minikel, E.V., Samocha, K.E., Banks, E., Fennell, T., O'Donnell-Luria, A.H., Ware, J.S., Hill, A.J., Cummings, B.B., et al.; Exome Aggregation Consortium (2016). Analysis of protein-coding genetic variation in 60,706 humans. Nature *536*, 285–291.
7. Schueler, M., Braun, D.A., Chandrasekar, G., Gee, H.Y., Klasson, T.D., Halbritter, J., Bieder, A., Porath, J.D., Airik, R., Zhou, W., et al. (2015). DCDC2 mutations cause a renal-hepatic ciliopathy by disrupting Wnt signaling. Am. J. Hum. Genet. *96*, 81–92.
8. Vivante, A., Kleppa, M.J., Schulz, J., Kohl, S., Sharma, A., Chen, J., Shril, S., Hwang, D.Y., Weiss, A.C., Kaminski, M.M., et al. (2015). Mutations in TBX18 Cause Dominant Urinary Tract Malformations via Transcriptional Dysregulation of Ureter Development. Am. J. Hum. Genet. *97*, 291–301.
9. Li, H., Handsaker, B., Wysoker, A., Fennell, T., Ruan, J., Homer, N., Marth, G., Abecasis, G., Durbin, R.; and 1000 Genome Project Data Processing Subgroup (2009). The Sequence Alignment/Map format and SAMtools. Bioinformatics *25*, 2078–2079.
10. Van der Auwera, G.A., Carneiro, M.O., Hartl, C., Poplin, R., Del Angel, G., Levy-Moonshine, A., Jordan, T., Shakir, K., Roazen, D., Thibault, J., et al. (2013). From FastQ data to high confidence variant calls: the Genome Analysis Toolkit best practices pipeline. Curr. Protoc. Bioinformatics *43*, 1–33.
11. Seelow, D., Schuelke, M., Hildebrandt, F., and Nürnberg, P. (2009). HomozygosityMapper–an interactive approach to homozygosity mapping. Nucleic Acids Res. *37*, W593–W599.
12. Hildebrandt, F., Heeringa, S.F., Rüschendorf, F., Attanasio, M., Nürnberg, G., Becker, C., Seelow, D., Huebner, N., Chernin, G., Vlangos, C.N., et al. (2009). A systematic approach to mapping recessive disease genes in individuals from outbred populations. PLoS Genet. *5*, e1000353.
13. Sobreira, N., Schiettecatte, F., Valle, D., and Hamosh, A. (2015). GeneMatcher: a matching tool for connecting investigators with an interest in the same gene. Hum. Mutat. *36*, 928–930.
14. Borck, G., Hög, F., Dentici, M.L., Tan, P.L., Sowada, N., Medeira, A., Gueneau, L., Thiele, H., Kousi, M., Lepri, F., et al. (2015). BRF1 mutations alter RNA polymerase III-dependent transcription and cause neurodevelopmental anomalies. Genome Res. *25*, 155–166.
15. Niceta, M., Stellacci, E., Gripp, K.W., Zampino, G., Kousi, M., Anselmi, M., Traversa, A., Ciolfi, A., Stabley, D., Bruselles, A., et al. (2015). Mutations Impairing GSK3-Mediated MAF Phosphorylation Cause Cataract, Deafness, Intellectual Disability, Seizures, and a Down Syndrome-like Facies. Am. J. Hum. Genet. *96*, 816–825.
16. Bolar, N.A., Golzio, C., Živná, M., Hayot, G., Van Hemelrijk, C., Schepers, D., Vandeweyer, G., Hoischen, A., Huyghe, J.R., Raes, A., et al. (2016). Heterozygous Loss-of-Function SEC61A1 Mutations Cause Autosomal-Dominant Tubulo-Interstitial and Glomerulocystic Kidney Disease with Anemia. Am. J. Hum. Genet. *99*, 174–187.
17. Isrie, M., Breuss, M., Tian, G., Hansen, A.H., Cristofoli, F., Morandell, J., Kupchinsky, Z.A., Sifrim, A., Rodriguez-Rodriguez, C.M., Dapena, E.P., et al. (2015). Mutations in Either TUBB or MAPRE2 Cause Circumferential Skin Creases Kunze Type. Am. J. Hum. Genet. *97*, 790–800.
18. Bögershausen, N., Tsai, I.C., Pohl, E., Kiper, P.O., Beleggia, F., Percin, E.F., Keupp, K., Matchan, A., Milz, E., Alanay, Y., et al. (2015). RAP1-mediated MEK/ERK pathway defects in Kabuki syndrome. J. Clin. Invest. *125*, 3585–3599.
19. Wortmann, S.B., Ziętkiewicz, S., Kousi, M., Szklarczyk, R., Haack, T.B., Gersting, S.W., Muntau, A.C., Rakovic, A., Renkema, G.H., Rodenburg, R.J., et al. (2015). CLPB mutations cause 3-methylglutaconic aciduria, progressive brain atrophy, intellectual disability, congenital neutropenia, cataracts, movement disorder. Am. J. Hum. Genet. *96*, 245–257.
20. Magini, P., Pippucci, T., Tsai, I.C., Coppola, S., Stellacci, E., Bartoletti-Stella, A., Turchetti, D., Graziano, C., Cenacchi, G., Neri, I., et al. (2014). A mutation in PAK3 with a dual molecular effect deregulates the RAS/MAPK pathway and drives an X-linked syndromic phenotype. Hum. Mol. Genet. *23*, 3607–3617.
21. Wan, J., Yourshaw, M., Mamsa, H., Rudnik-Schöneborn, S., Menezes, M.P., Hong, J.E., Leong, D.W., Senderek, J., Salman, M.S., Chitayat, D., et al. (2012). Mutations in the RNA exosome component gene EXOSC3 cause pontocerebellar hypoplasia and spinal motor neuron degeneration. Nat. Genet. *44*, 704–708.
22. Niederriter, A.R., Davis, E.E., Golzio, C., Oh, E.C., Tsai, I.C., and Katsanis, N. (2013). In vivo modeling of the morbid human genome using Danio rerio. J. Vis. Exp. (78), e50338.

23. Schulte, E.C., Kousi, M., Tan, P.L., Tilch, E., Knauf, F., Lichtner, P., Trenkwalder, C., Högl, B., Frauscher, B., Berger, K., et al. (2014). Targeted resequencing and systematic in vivo functional testing identifies rare variants in MEIS1 as significant contributors to restless legs syndrome. Am. J. Hum. Genet. *95*, 85–95.
24. Sarparanta, J., Jonson, P.H., Golzio, C., Sandell, S., Luque, H., Screen, M., McDonald, K., Stajich, J.M., Mahjneh, I., Vihola, A., et al. (2012). Mutations affecting the cytoplasmic functions of the co-chaperone DNAJB6 cause limb-girdle muscular dystrophy. Nat. Genet. *44*, 450–455.
25. Zhu, X., Xu, Y., Yu, S., Lu, L., Ding, M., Cheng, J., Song, G., Gao, X., Yao, L., Fan, D., et al. (2014). An efficient genotyping method for genome-modified animals and human cells generated with CRISPR/Cas9 system. Sci. Rep. *4*, 6420.
26. Matak, P., Zumerle, S., Mastrogiannaki, M., El Balkhi, S., Delga, S., Mathieu, J.R., Canonne-Hergaux, F., Poupon, J., Sharp, P.A., Vaulont, S., and Peyssonnaux, C. (2013). Copper deficiency leads to anemia, duodenal hypoxia, upregulation of HIF-2α and altered expression of iron absorption genes in mice. PLoS ONE *8*, e59538.
27. Müller, A., MacCallum, R.M., and Sternberg, M.J. (2002). Structural characterization of the human proteome. Genome Res. *12*, 1625–1641.
28. Huang, L., Szymanska, K., Jensen, V.L., Janecke, A.R., Innes, A.M., Davis, E.E., Frosk, P., Li, C., Willer, J.R., Chodirker, B.N., et al. (2011). TMEM237 is mutated in individuals with a Joubert syndrome related disorder and expands the role of the TMEM family at the ciliary transition zone. Am. J. Hum. Genet. *89*, 713–730.
29. Roberson, E.C., Dowdle, W.E., Ozanturk, A., Garcia-Gonzalo, F.R., Li, C., Halbritter, J., Elkhartoufi, N., Porath, J.D., Cope, H., Ashley-Koch, A., et al. (2015). TMEM231, mutated in orofaciodigital and Meckel syndromes, organizes the ciliary transition zone. J. Cell Biol. *209*, 129–142.
30. Deng, H.X., Shi, Y., Yang, Y., Ahmeti, K.B., Miller, N., Huang, C., Cheng, L., Zhai, H., Deng, S., Nuytemans, K., et al. (2016). Identification of TMEM230 mutations in familial Parkinson's disease. Nat. Genet. *48*, 733–739.
31. Valente, E.M., Logan, C.V., Mougou-Zerelli, S., Lee, J.H., Silhavy, J.L., Brancati, F., Iannicelli, M., Travaglini, L., Romani, S., Illi, B., et al. (2010). Mutations in TMEM216 perturb ciliogenesis and cause Joubert, Meckel and related syndromes. Nat. Genet. *42*, 619–625.
32. Lee, J.H., Silhavy, J.L., Lee, J.E., Al-Gazali, L., Thomas, S., Davis, E.E., Bielas, S.L., Hill, K.J., Iannicelli, M., Brancati, F., et al. (2012). Evolutionarily assembled cis-regulatory module at a human ciliopathy locus. Science *335*, 966–969.
33. Foulquier, F., Amyere, M., Jaeken, J., Zeevaert, R., Schollen, E., Race, V., Bammens, R., Morelle, W., Rosnoblet, C., Legrand, D., et al. (2012). TMEM165 deficiency causes a congenital disorder of glycosylation. Am. J. Hum. Genet. *91*, 15–26.
34. Merner, N.D., Hodgkinson, K.A., Haywood, A.F., Connors, S., French, V.M., Drenckhahn, J.D., Kupprion, C., Ramadanova, K., Thierfelder, L., McKenna, W., et al. (2008). Arrhythmogenic right ventricular cardiomyopathy type 5 is a fully penetrant, lethal arrhythmic disorder caused by a missense mutation in the TMEM43 gene. Am. J. Hum. Genet. *82*, 809–821.
35. Gherman, A., Davis, E.E., and Katsanis, N. (2006). The ciliary proteome database: an integrated community resource for the genetic and functional dissection of cilia. Nat. Genet. *38*, 961–962.
36. Badano, J.L., Mitsuma, N., Beales, P.L., and Katsanis, N. (2006). The ciliopathies: an emerging class of human genetic disorders. Annu. Rev. Genomics Hum. Genet. *7*, 125–148.